Super-resolution in confocal scanning microscopy. V. Axial super-resolution in the incoherent case

1994 Inverse Problems 10 1059

(http://iopscience.iop.org/0266-5611/10/5/005)

Inverse Problems 10 (1994) 1059–1077. Printed in the UK

Super-resolution in confocal scanning microscopy: V. Axial super-resolution in the incoherent case

M Bertero†, P Boccacci†, F Malfanti‡ and E R Pike§

† Dipartimento di Fisica, Università di Genova and INFN, Via Dodecaneso 33, I-16146 Genova, Italy

‡ Dipartimento di Scienze della Terra, Università di Genova, Viale Benedetto XV 5, I-16132 Genova, Italy

§ Department of Physics, King's College, Strand, London WC2R 2LS, UK

Received 24 March 1994

Abstract. One of the basic properties of confocal scanning laser microscopy (CSLM) is the possibility of high axial resolution in the case of fluorescent objects. As a consequence 3D images of 3D objects can be obtained. In the previous papers of this series it has been demonstrated that an improvement of lateral resolution in CSLM (lateral super-resolution) can be obtained if, at each step of the scanning procedure, the full image is detected in the image plane and these data are inverted to estimate the object at the confocal point. In this paper we prove that the same data contain sufficient information for improving also the axial resolution of CSLM (axial super-resolution). The analysis is performed in the case of a simplified model, i.e. two-dimensional objects (one lateral plus one axial dimension) and lenses with a small numerical aperture.

1. Introduction

The possibility of super-resolution in confocal scanning laser microscopy (CSLM) has been demonstrated in both the coherent [1] and incoherent [2] cases (fluorescence microscopy). These results, obtained for one-dimensional pupils, have also been extended to circular pupils [3]. The method requires that the full image is measured, by means of a suitable array of detectors, at each step of the scanning procedure. In a recent paper [4], however, it has been shown that the array of detectors can be conveniently replaced by a suitable holographic mask and experimental confirmation has been achieved in both the coherent [5] and incoherent [6] cases.

The papers mentioned above demonstrate the improvement of resolution, with respect to conventional CSLM, in the direction orthogonal to the optical axis of the instrument (lateral resolution). It is well known, however, that one of the interesting properties of CSLM is the optical sectioning of a fluorescent object [7, 8]. As a result three-dimensional imaging of biological objects becomes possible. A difficulty is that these images are orientation dependent since the lateral resolution is better than the axial resolution. Such a difficulty would be increased by super-resolving CSLM if this new technique could improve lateral resolution only. Therefore it is important to investigate the effect of the measurement of the full image on the axial resolution. An indication of axial super-resolution has already been obtained by means of numerical computations in the case of lenses with high numerical aperture (NA) [9]. These computations are still very preliminary and not very accurate. The reason is that the computation of the matrix that approximates the integral operator is time consuming: each matrix element is given by a double integral. As a consequence it has only

0266-5611/94/051059+19$19.50

been possible to use matrices of moderate size. The purpose of this paper is to investigate carefully the problem in a rather simplified situation, namely in the case where the objects depend on only one lateral variable and the numerical aperture of the lenses is small. In this case we do not have the difficulty mentioned for the high NA problem.

In general, if we consider a three-dimensional fluorescent object and if $f(\rho; z)$ (where $\rho = \{x, y\}$) is the distribution function of the fluorescent centres (here the origin of the coordinate system is the confocal point and the z axis coincides with the optical axis of the microscope so that the plane $z = 0$ is the confocal plane of the system) then the intensity distribution in the image plane is given by [9]

$$g(\rho) = \int W(|\rho - \rho'|; z')W(\rho'; z')f(\rho'; z')\,\mathrm{d}\rho'\,\mathrm{d}z' \tag{1.1}$$

where $W(\rho; z)$ is the time-averaged electrical energy distribution in the focal region. This equation is valid under the following assumptions:

(i) the optical system is invariant with respect to rotations around the optical axis;
(ii) the excitation light is circularly polarized;
(iii) the fluorescent material is weakly absorbing;
(iv) the fluorescent radiation is completely incoherent and randomly polarized;
(v) the difference between the wavelength of the excitation radiation and the wavelength of the fluorescent radiation is neglected.

In the case of objects which depend on only one lateral variable (let us say the x variable) and for cylindrical lenses, (1.1) takes the form

$$g(x) = \int_{-\infty}^{+\infty} \mathrm{d}x' \int_{-\infty}^{+\infty} \mathrm{d}z'\, W(x - x', z')W(x', z')f(x', z'). \tag{1.2}$$

A further simplification is obtained if we assume that the numerical aperture of the objectives is small. In this case we can use the scalar theory of diffraction and the function $W(x, z)$ is given by

$$W(x, z) = |S(x, z)|^2 \tag{1.3}$$

where

$$S(x, z) = \tfrac{1}{2}\int_{-1}^{1} \exp\{-\mathrm{i}\pi(xt + \tfrac{1}{2}zt^2)\}\,\mathrm{d}t. \tag{1.4}$$

This expression can be easily derived from the Debye integral [10]. We point out that the coordinates x, z are essentially optical coordinates, related to the geometrical coordinates x_0, z_0 by the relations

$$x = \frac{2}{\lambda}\left(\frac{a}{f}\right)x_0 \qquad z = \frac{2}{\lambda}\left(\frac{a}{f}\right)^2 z_0 \tag{1.5}$$

where a is the half-width of the cylindrical lenses, f is the common focal length and λ is the wavelength of the radiation. This choice is equivalent to taking the lateral Rayleigh resolution distance as the unit of length. We also point out that the normalization of the function $S(x, z)$ has been chosen in such a way that

$$S(x, 0) = \mathrm{sinc}(x) \tag{1.6}$$

where

$$\operatorname{sinc}(x) = \frac{\sin(\pi x)}{\pi x}. \tag{1.7}$$

Therefore, when $f(x,z) = f(x)\delta(z)$, the integral equation (1.2) coincides with the integral equation investigated in [2].

As in [1,2] we must solve the following problem: given $g(x)$, estimate the value of $f(x,z)$ at the point $x = z = 0$. This problem must be solved for each scanning position, the two-dimensional image being obtained by means of a two-dimensional scanning (both in the x direction and in the z direction). We recall that in the conventional CSLM only the value of the image at the confocal point, i.e. $g(0)$, is detected at each scanning position and therefore, if one neglects the integration effect of the pinhole, the impulse response function of the conventional CSLM is given by

$$T(x,z) = |W(x,z)|^2. \tag{1.8}$$

The effect of the pinhole, however, must be taken into account in estimating the resolution which can be achieved in practice. For this reason we will not neglect the pinhole when we compare the impulse response function of the conventional CSLM with that of the super-resolving one.

In section 2 we investigate the main properties of the integral operator (1.2), in particular we prove that it is compact, so that we can introduce its singular system. In section 3 we present both a discretization of the integral equation based on the sampling theorem and a discretization obtained by taking the Fourier transform of (1.2) with respect to the x variable. This is used for computing approximations both of the singular values and of the singular functions. In section 4 we discuss the numerical results we have obtained concerning the singular system of the integral operator (1.2). In section 5 we demonstrate the possibility of axial super-resolution and we compare the results presented in this paper with the results given in [2].

2. The integral operator

The integral equation (1.2) can be written in the form

$$g = Af \tag{2.1}$$

where A is the integral operator

$$(Af)(x) = \int_{-\infty}^{+\infty} \mathrm{d}x' \int_{-\infty}^{+\infty} \mathrm{d}z'\, W(x-x',z')W(x',z')f(x',z') \tag{2.2}$$

the function $W(x,z)$ being defined by (1.3) and (1.4).

The operator A transforms a function of two variables into a function of one variable. It will be considered as an operator from $L^2(\mathbb{R}^2)$ into $L^2(\mathbb{R})$.

Our first result is the following: the operator $A : L^2(\mathbb{R}^2) \to L^2(\mathbb{R})$ is of the Hilbert–Schmidt class and therefore it is compact.

In order to prove this result let us first remark that the function

$$\sigma(z) = \int_{-\infty}^{+\infty} |W(x,z)|^2 \,\mathrm{d}x = \int_{-\infty}^{+\infty} T(x,z)\,\mathrm{d}x \tag{2.3}$$

is square integrable since, for large z, it is bounded by

$$\sigma(z) \leqslant \text{constant}/|z|. \tag{2.4}$$

In fact, from the bounds (A.7), (A.8) for $S(x, z)$ (see appendix A), it follows that, for $z > 0$

$$\begin{aligned}\sigma(z) &= \int_{|x|\leqslant z} |S(x,z)|^4\,\mathrm{d}x + \int_{|x|\geqslant z} |S(x,z)|^4\,\mathrm{d}x \\ &\leqslant \frac{2C_1^4}{z} + 2C_2^4 \int_z^{+\infty} \frac{\mathrm{d}x}{x^4} = \frac{2C_1^4}{z} + \frac{2}{3}\frac{C_2^4}{z^3}\end{aligned} \tag{2.5}$$

and this implies the bound (2.4) if we notice that $\sigma(-z) = \sigma(z)$. An estimate of the constant in (2.4) can be obtained if we notice that, from (B.5) and the Parseval equality, we have

$$\sigma(z) = \frac{1}{\pi z^2} \int_0^{2\pi} \frac{\sin^2\left[\xi(1-\xi/2\pi)z\right]}{\xi^2}\,\mathrm{d}\xi. \tag{2.6}$$

Then, by a suitable estimate of the integral, we get

$$\sigma(z) \leqslant \frac{2}{\pi|z|} \qquad |z| \geqslant \frac{1}{2\pi}. \tag{2.7}$$

Finally, an elementary change of variables shows that

$$\begin{aligned}\| A \|_{\mathrm{HS}}^2 &= \int_{-\infty}^{+\infty} \mathrm{d}x \int_{-\infty}^{+\infty} \mathrm{d}x' \int_{-\infty}^{+\infty} \mathrm{d}z'\, |W(x-x',z')|^2 |W(x',z')|^2 \\ &= \int_{-\infty}^{+\infty} \sigma^2(z')\,\mathrm{d}z' \\ &< +\infty\end{aligned} \tag{2.8}$$

and therefore the operator A is of the Hilbert–Schmidt class.

We recall that the singular system of A is the set of the triples $\{\alpha_k; u_k, v_k\}$ which solve the shifted eigenvalue problem

$$Au_k = \alpha_k v_k \qquad A^* v_k = \alpha_k u_k \tag{2.9}$$

where A^* is the adjoint of the operator A. It is given by

$$(A^* g)(x', z') = W(x', z') \int_{-\infty}^{+\infty} W(x - x', z') g(x)\,\mathrm{d}x. \tag{2.10}$$

We notice that this operator transforms a function of one variable into a function of two variables and it is a compact operator from $L^2(\mathbb{R})$ into $L^2(\mathbb{R}^2)$.

Some properties of the singular functions can be inferred just by observing that the u_k are in the range of the operator A^*, while the v_k are in the range of the operator A. For this purpose we recall that the function $S(x, z)$ (see appendix A) as well as the functions $W(x, z)$

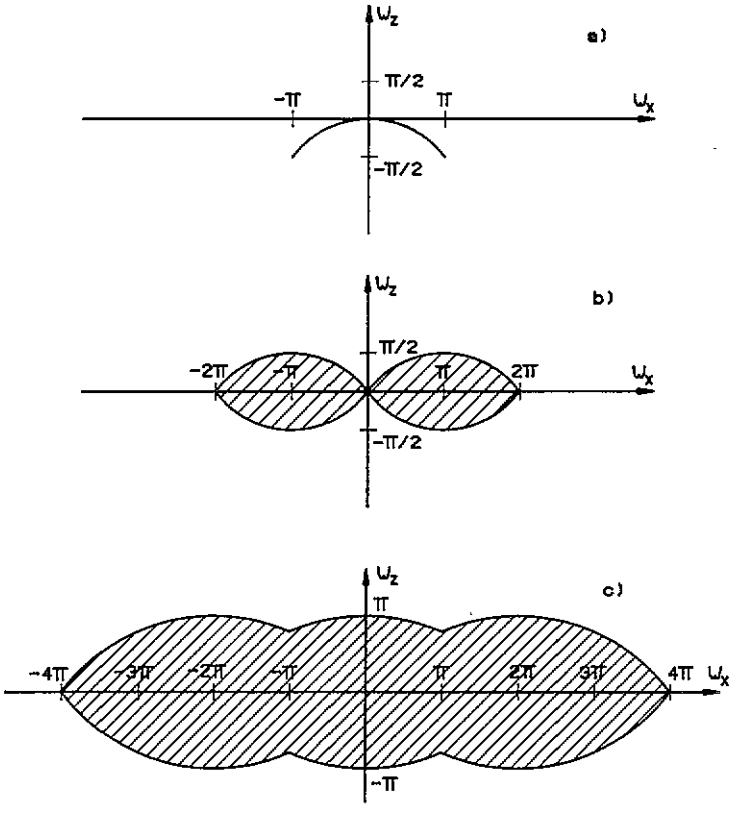

Figure 1. Supports of the functions (*a*) $\hat{S}(\omega_x, \omega_z)$, (*b*) $\hat{W}(\omega_x, \omega_z)$ and (*c*) $\hat{T}(\omega_x, \omega_z)$.

and $T(x, z)$ are band limited (see appendix B). The supports of their Fourier transforms (FT) $\hat{S}(\omega_x, \omega_z)$, $\hat{W}(\omega_x, \omega_z)$ and $\hat{T}(\omega_x, \omega_z)$ are given in figure 1.

Then we have the following properties of the singular functions u_k:

(a) they are functions of two variables x, z and even functions of z;
(b) they are band limited and the support of $\hat{u}_k(\omega_x, \omega_z)$ is interior to the support of $\hat{T}(\omega_x, \omega_z)$ (see figure 1);
(c) they form an orthonormal basis in the closure of the range of A^*, which is the orthogonal complement of the null space, $N(A)$, of the operator A.

As concerns the singular functions v_k, we have that:

(a′) they are functions of only one variable, x;
(b′) they are band limited and their support is interior to the interval $[-2\pi, 2\pi]$;
(c′) they form an orthonormal basis in the closure of the range of A, which is the orthogonal complement of the null space, $N(A^*)$, of the operator A.

Since $N(A)$ is not trivial (it contains, at least, all the functions whose FT is zero over the band of $T(x, z)$, figure 1), the solution of (2.1) is not unique. The generalized solution of this equation is the unique least-squares solution orthogonal to $N(A)$. As a consequence it belongs to the closure of the range of A^*. In terms of the singular system it is given by

$$f^+(x', z') = \sum_{k=0}^{+\infty} \frac{1}{\alpha_k} (g, v_k)_1 u_k(x', z') \tag{2.11}$$

where $(g, v_k)_1$ denotes the scalar product in $L^2(\mathbb{R})$. This is an even function of z'. However, we are only interested in estimating f^+ at the confocal point, $x' = z' = 0$.

3. Discretization of the integral equation

The method used in [2–4] for discretizing the integral equations of confocal microscopy was based on the sampling theorem and can be extended to the present case. In fact, the functions in the range of the integral operator A, equation (2.2), are band limited, with a band interior to the interval $[-2\pi, 2\pi]$ and therefore they can be represented by means of the sampling expansion

$$g(x) = \sum_{n=-\infty}^{+\infty} g(\tfrac{1}{2}n)\,\mathrm{sinc}[2(x - \tfrac{1}{2}n)] \tag{3.1}$$

the function $\mathrm{sinc}(x)$ being defined as in (1.7). On the other hand, the generalized solution (2.9) is in the range of the integral operator A^*, equation (2.10), and therefore is also bandlimited, with a band interior to the rectangle

$$|\omega_x'| \leqslant 4\pi \qquad |\omega_z'| \leqslant \pi \tag{3.2}$$

(see figure 1). Therefore we can restrict (2.1) to this subspace, whose functions can be represented by means of the sampling expansion

$$f(x', z') = \sum_{m=-\infty}^{+\infty} \sum_{l=-\infty}^{+\infty} f(\tfrac{1}{4}m, l)\,\mathrm{sinc}[4(x' - \tfrac{1}{4}m)]\,\mathrm{sinc}(z' - l). \tag{3.3}$$

We also notice that the following relations hold

$$\int_{-\infty}^{+\infty} |g(x)|^2\,\mathrm{d}x = \tfrac{1}{2} \sum_{n=-\infty}^{+\infty} \left|g(\tfrac{1}{2}n)\right|^2 \tag{3.4}$$

$$\int\int_{-\infty}^{+\infty} |f(x', z')|^2\,\mathrm{d}x'\,\mathrm{d}z' = \tfrac{1}{4} \sum_{m=-\infty}^{+\infty} \sum_{l=-\infty}^{+\infty} \left|f(\tfrac{1}{4}m, l)\right|^2. \tag{3.5}$$

Now, the singular functions $v_k(x)$ are in the range of the operator A and therefore they can be represented by means of the sampling expansion (3.1), while the singular functions $u_k(x', z')$ are in the range of the operator A^* and therefore they can be represented by means of the sampling expansion (3.3). This remark implies the equivalence, from the point of view of the computation of the singular system, between the original integral equation and the infinite-dimensional linear system obtained by inserting the sampling expansions in the integral equation. The procedure is completely analogous to that followed in [2, 3] and therefore we do not give the details of the derivation.

If we introduce the coefficients

$$b_n = \frac{1}{\sqrt{2}} g\left(\frac{n}{2}\right) \qquad a_{m,l} = \frac{1}{2} f\left(\frac{m}{4}, l\right) \tag{3.6}$$

then the final result is

$$b_n = \sum_{m,l=-\infty}^{+\infty} A_{n;m,l} a_{m,l} \tag{3.7}$$

where

$$A_{n;m,l} = \frac{1}{2^{3/2}} W\left(\frac{n}{2} - \frac{m}{4}, l\right) W\left(\frac{m}{4}, l\right). \tag{3.8}$$

The singular values of the infinite-dimensional matrix (3.8) coincide with the singular values of the integral operator (2.2). Approximations of these singular values can be computed by considering finite sections of the matrix (3.8) obtained by limiting the values of the indices as follows

$$n = 0, \pm 1, \ldots, \pm N \qquad m = 0, \pm 1, \ldots, \pm M \qquad l = 0, \pm 1, \ldots, \pm L. \tag{3.9}$$

We will also write, as in [2]

$$N_0 = 2N + 1 \qquad M_0 = 2M + 1 \qquad L_0 = 2L + 1. \tag{3.10}$$

When $N_0, M_0, L_0 \to \infty$, the singular values of the finite-dimensional matrix converge to the singular values of the infinite-dimensional one. Moreover, if we denote by $U_{m,l}^{(k)}$ and $V_n^{(k)}$ the components of the singular vectors of the finite-dimensional matrix (normalized to one with respect to the usual Euclidean norm), from (3.6) and the truncated sampling expansions, we obtain the following approximations to the singular functions of the integral operator (2.2)

$$v_k(x) = \sqrt{2} \sum_{n=-N}^{N} V_n^{(k)} \operatorname{sinc}[2(x - \tfrac{1}{2}n)] \tag{3.11}$$

$$u_k(x', z') = 2 \sum_{m=-M}^{M} \sum_{l=-L}^{L} U_{m,l}^{(k)} \operatorname{sinc}[4(x' - \tfrac{1}{4}m)] \operatorname{sinc}(z' - l). \tag{3.12}$$

Computations have been performed for several values of N_0, M_0 and L_0, trying to check the convergence of the procedure. It is the case that the convergence is much slower than that of the one-dimensional problem considered in [2]. This is due to a poor evaluation of the two-dimensional integral by means of the sampling expansion as a consequence of the behaviour at infinity of the function $W(x, z)$ (see appendix A).

The maximum values of N_0, M_0 and L_0 we have considered are $N_0 = 193$ (i.e. sampling points in the interval $[-48, 48]$); $M_0 = 1537$ and $L_0 = 385$ (the choices of M_0 and L_0 correspond to sampling points in the interval $[-192, 192]$ both for x' and z'). Since these figures correspond to a matrix $[A]$ which is $N_0 \times (M_0 L_0)$, the singular values have been computed as square roots of the eigenvalues of the matrix $[A][A]^{\mathrm{T}}$ which is only $N_0 \times N_0$. The matrix elements (3.8) have been obtained by producing a table of the values of the function $W(\frac{1}{4}m, l)$ (each of them implies the computation of a one-dimensional integral).

The previous method requires time consuming computations and the results are not completely satisfactory. In particular, the transfer functions (see the next section) obtained in this way show some oscillatory structures which come from the truncation of the sampling

expansions. For this reason we have also considered an alternative method already used in [4].

We take the Fourier transform of both sides of (1.2) and denote by $\hat{g}(\omega_x)$ the Fourier transform of $g(x)$ and by $\tilde{W}(\omega_x, z)$ and $\tilde{f}(\omega_x, z)$ the Fourier transform, with respect to x for z fixed, of $W(x, z)$ and $f(x, z)$, respectively. Then, from the convolution theorem we get

$$\hat{g}(\omega_x) = \frac{1}{2\pi} \int_{-\infty}^{+\infty} dz' \, \tilde{W}(\omega_x, z') \int_{\omega_x - 2\pi}^{\omega_x + 2\pi} d\omega_x' \, \tilde{W}(\omega_x - \omega_x', z') \tilde{f}(\omega_x', z') \tag{3.13}$$

for $|\omega_x| < 2\pi$ and $\hat{g}(\omega_x) = 0$ elsewhere. In fact, as follows from (B.5), $\tilde{W}(\omega_x, z) = 0$ when $|\omega_x| > 2\pi$. The advantage of (3.13) over (1.2) is that it is an equation on a bounded interval, as concerns the variable ω_x, and that the function $\tilde{W}(\omega_x, z')$ is elementary (see (B.5)) so that its evaluation does not require the computation of an integral.

Now, the function $\tilde{W}(\omega_x, z')$ is band limited, as a function of z; its bandwidth depends on ω_x and is given by (see (B.5)): $\Omega = |\omega_x|(1 - |\omega_x|/2\pi) < \frac{1}{2}\pi$. On the other hand, if we look for the generalized solution of (3.13), this is a band limited function of z', with a bandwidth smaller than π.

Therefore, we can represent $\tilde{f}(\omega_x', z')$ by the following sampling expansion

$$\tilde{f}(\omega_x', z') = \sum_{l=-\infty}^{+\infty} \tilde{f}(\omega_x', l) \operatorname{sinc}(z' - l) \tag{3.14}$$

and if we substitute this expansion in (3.13) we get

$$\hat{g}(\omega_x) = \frac{1}{2\pi} \sum_{l=-\infty}^{+\infty} \tilde{W}(\omega_x, l) \int_{\omega_x - 2\pi}^{\omega_x + 2\pi} \tilde{W}(\omega_x - \omega_x', l) \tilde{f}(\omega_x', l) \, d\omega_x'. \tag{3.15}$$

The integral with respect to ω_x' can be discretized by means of a simple trapezoidal rule. In order to have the same distance between discrete points both in ω_x and in ω_x', we must take $2N + 1$ points for $\omega_x \in [-2\pi, 2\pi]$ and $4N + 1$ points for $\omega_x' \in [-4\pi, 4\pi]$. In both cases the distance between adjacent points is $\delta = 2\pi/N$. Therefore, if we take into account the relationship between sampling distance in the ω_x variable and the length of the interval of the x variable, the discretization of the variables ω_x and ω_x' corresponds to restricting the x and x' variables to the interval $[-\frac{1}{2}N, \frac{1}{2}N]$.

Since $\tilde{W}(\omega_x, l) = 0$ when $|\omega_x| \geqslant 2\pi$, we have $\hat{g}(\pm 2\pi) = 0$; moreover, the sampled values $\tilde{f}[\pm(4\pi - s\delta), l]$ $(s = 0, 1)$ do not appear in the equation. As a consequence we can use only $2N - 1$ points in the ω_x variable

$$\omega_n = -2\pi + \frac{2\pi}{N}(n + 1) \qquad n = 0, 1, 2, \ldots, 2N - 2 \tag{3.16}$$

and $4N - 3$ points in the ω_x' variable

$$\omega_m' = -4\pi + \frac{2\pi}{N}(m + 2) \qquad m = 0, 1, 2, \ldots, 4N - 4. \tag{3.17}$$

As concerns the truncation of the sum with respect to l in (3.15), we observe that this truncation depends on the discretization of the ω variables. In fact the distance of the first

zero of the function $\tilde{W}(\omega_x, l)$ from the origin is approximately $|\omega_x| = \pi/|l|$ and therefore the maximum value of $|l|$, which we denote by L, must be such that

$$\frac{\pi}{L} > \delta = \frac{2\pi}{N} \tag{3.18}$$

i.e. $L < \frac{1}{2}N$. Finally the discrete form of (3.15) will be

$$\hat{g}(\omega_n) = \sum_{l=-L}^{L} \sum_{m=0}^{4N-4} A_{n;m,l} \tilde{f}(\omega'_m, l) \qquad n = 0, 1, \ldots, 2N-2$$

where, taking into account that $\tilde{W}(\omega_n - \omega'_m, l) = 0$ whenever $|\omega_n - \omega'_m| \geqslant 2\pi$, we have

$$A_{n;m,l} = \begin{cases} \dfrac{1}{N} \tilde{W}(\omega_n, l) \tilde{W}(\omega_n - \omega'_m, l) \\ \qquad n = 0, 1, \ldots, 2N-2, \ m = n, n+1, \ldots, n+2N-2 \\ 0 \qquad \text{elsewhere} . \end{cases} \tag{3.19}$$

In this case the singular system $\{\alpha_k; U^{(k)}, V^{(k)}\}$ of A is also computed by diagonalizing the matrix AA^{T}. If the singular vectors $U^{(k)}$ and $V^{(k)}$ are normalized with respect to the Euclidean norm, then the corresponding approximations of the singular functions $u_k(x, z)$ and $v_k(x)$, normalized with respect to the L^2-norm can be obtained as follows

$$v_k(x) = \frac{1}{\sqrt{N}} \sum_{n=0}^{2N-2} e^{ix\omega_n} V_n^{(k)}. \tag{3.20}$$

$$u_k(x', z') = \frac{1}{\sqrt{N}} \sum_{m=0}^{4N-4} e^{ix'\omega'_m} \sum_{l=-L}^{L} U_{m,l}^{(k)} \operatorname{sinc}(z' - l). \tag{3.21}$$

It is obvious that, although we have used the same notation, the singular vectors appearing in (3.20) and (3.21) are different from the singular vectors of (3.11) and (3.12).

In the case of the matrix (3.19), we have also computed the singular system for various values of N and L up to $N = 220$ and $L = 50$. If we introduce the total numbers of values of the indices n, m, l and we again call these N_0, M_0, L_0, we have now

$$N_0 = 2N - 1 \qquad M_0 = 4N - 3 \qquad L_0 = 2L + 1. \tag{3.22}$$

Therefore the maximum values considered have been $N_0 = 439$, $M_0 = 877$ and $L_0 = 101$. These correspond to the interval $[-110, 110]$ for the x and x' variables and to the interval $[-50, 50]$ for the z' variable.

4. The singular system: numerical results

The singular system of the matrix (3.8) or of the matrix (3.19) has been computed for various values of the parameters N_0, M_0 and L_0. We have verified that, by increasing these parameters, the convergence of the singular values is rather slow. Anyway we believe that at least three of four digits are correct for the largest singular values, let us say the first ten

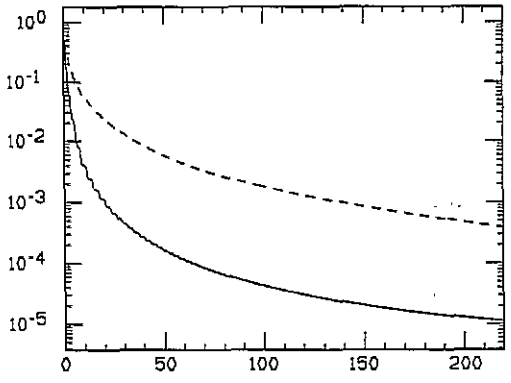

Figure 2. The singular values α_k as a function of k from $k = 0$ up to $k = 220$ (broken curve) on a semilogarithmic scale. The full curve represents the behaviour of α_k in the case of the 1D problem. Linear interpolation between adjacent singular values has been used in the representation.

singular values. Moreover, if we compare the singular values obtained by the two methods and corresponding, in both cases, to the maximum values of N_0, M_0 and L_0 specified in section 3, we find a difference which is smaller than 1% up to $k = 21$, between 1% and 10% up to $k = 50$, between 10% and 20% up to $k = 85$, and so on. For instance, the estimate of α_0 provided by the first method is $\alpha_0 = 0.915\,285$ while that provided by the second one is $\alpha_0 = 0.915\,212$. The other results we report in this section are those obtained by means of the second method of section 3.

The behaviour of the singular value spectrum in the case $N = 220$, $L = 50$ is shown in figure 2. In the same figure it is compared with the singular value spectrum of the 1D problem considered in [2] (full curve). It is obvious that the decay of the 2D spectrum is much slower than that of the 1D one. This implies that, for a given noise level, the number of degrees of freedom of the 2D problem is much greater than the number of degrees of freedom of the 1D problem. For instance in the 2D case we have 34 singular values greater than 10^{-2} (7 in the 1D case), 125 greater than 10^{-3} (21 in the 1D case) and 267 greater than 10^{-4} (64 in the 1D case). This result is just what should have been expected. Since the image is 1D in both cases and the instrument is operating in the same way, to invert data by assuming 1D objects instead of 2D ones, is equivalent to using *a priori* knowledge about the object in the inversion procedure. As is known, the use of *a priori* knowledge always implies a reduction of the number of degrees of freedom with respect to the case where no *a priori* knowledge is used.

We do not give figures showing the behaviour of the singular functions $v_k(x)$ and $u_k(x, z)$, we only describe some of their properties. As concerns the functions $v_k(x)$ they are alternatively even and odd and more precisely they are even when k is even and odd when k is odd, except for values of k from 3 to 8 where an inversion occurs. It is not clear if this is a numerical effect due to the approximations used for the computation of the singular values or if it is a property of the singular functions of the integral operator. Anyway, if we rearrange the singular functions $v_k(x)$ for these values of k in such a way that they are always alternatively even and odd, the Fourier transforms $\hat{v}_k(\omega_x)$ have another simple property. We already know that $\hat{v}_k(\pm 2\pi) = 0$ (see section 3); our numerical calculations show that $\hat{v}_k(\omega_x)$ ($k = 0, 1, 2, \ldots$) has exactly k zeros interior to the interval $(-2\pi, 2\pi)$.

As concerns the singular functions $u_k(x, z)$, we know that they are always even functions of z (see section 2). As a function of x, $u_k(x, z)$ has the same parity as $v_k(x)$, i.e. it is even if $v_k(x)$ is even and odd if $v_k(x)$ is odd. This is just a consequence of the second equation in (2.9). Moreover, $\hat{u}_k(\omega_x, \omega_z)$ can take large values in a neighbourhood of the point $\omega_x = \omega_z = 0$ and this is the numerical consequence of the singularity of the singular functions of the integral operator. This singularity is induced by the singularity at that point

of the function $\hat{T}(\omega_x, \omega_z)$ (see (B.9) and (B.11)). In particular, the behaviour of $\hat{u}_0(\omega_x, \omega_z)$ is quite similar to the behaviour of $\hat{T}(\omega_x, \omega_z)$, except for a normalization constant (see figure 4 in the next section).

The singular functions can be used for the computation of the optical masks introduced in [4]. If we use only K terms in the truncated singular function expansion of the solution, then the corresponding optical mask $M_K(x)$ is given by

$$M_K(x) = \sum_{k=0}^{K-1} \frac{1}{\alpha_k} u_k(0,0) v_k(x). \tag{4.1}$$

We have computed this function in three cases: (i) using all the singular values $> 10^{-2}$; (ii) using all the singular values $> 10^{-3}$; (iii) using all the singular values computed by the second method of section 3 with the maximum values of N_0, M_0 and L_0. Only the even singular functions $v_k(x)$ contribute to (4.1) because for the odd ones, the corresponding functions $u_k(x, z)$ are odd functions of x so that $u_k(0, 0) = 0$. It follows that

$$M_K(-x) = M_K(x) \tag{4.2}$$

and for this reason in figure 3 we represent $M_K(x)$ only for $x > 0$.

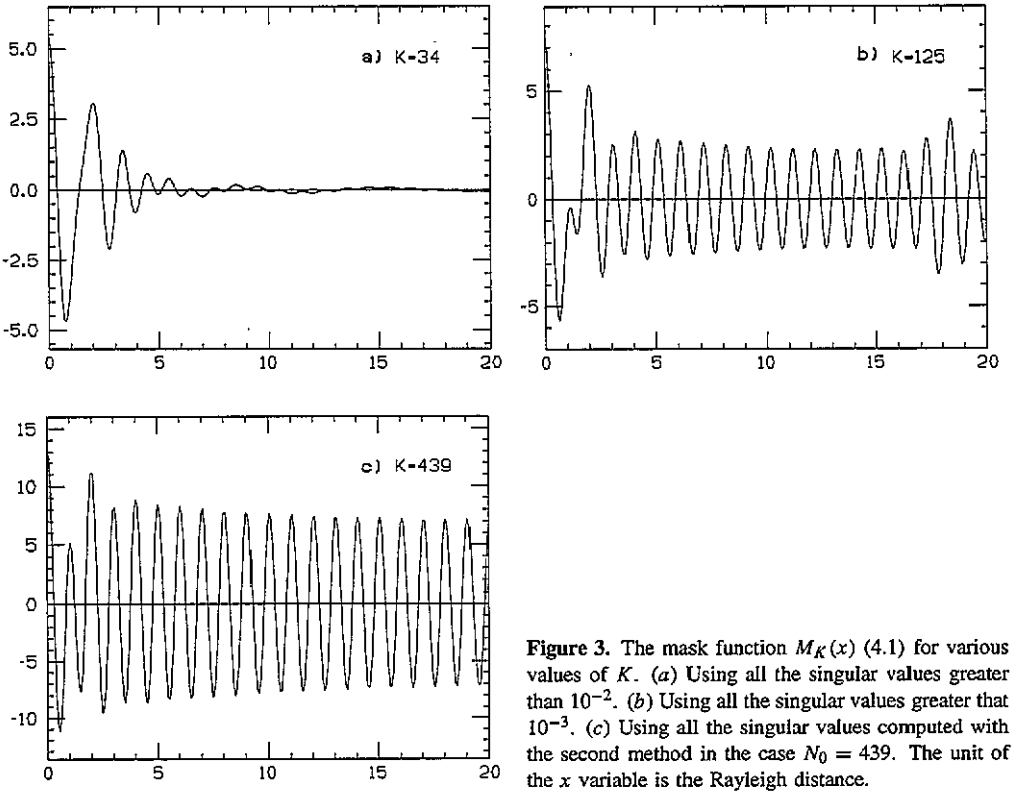

Figure 3. The mask function $M_K(x)$ (4.1) for various values of K. (*a*) Using all the singular values greater than 10^{-2}. (*b*) Using all the singular values greater that 10^{-3}. (*c*) Using all the singular values computed with the second method in the case $N_0 = 439$. The unit of the x variable is the Rayleigh distance.

We notice that, for increasing values of K, the behaviour of $M_K(x)$ becomes more and more regular; moreover, the maximum value of $|M_K(x)|$ does not diverge for increasing K as in the 1D incoherent case (see [4]). Therefore we can conjecture that $M_K(x)$ has a limit

when $K \to \infty$. This limit is presumably quite similar to the function shown in figure 3(*c*). We see that, except in a region close to $x = 0$ whose size is of the order of few Rayleigh distances, this function exhibits quite regular oscillations with uniformly spaced zeros, the distance between adjacent zeros being approximately half the Rayleigh distance.

5. The transfer function

As mentioned in the introduction, the imaging properties of the conventional CSLM can be described in terms of the *impulse response function* $T(x, z)$ given by (1.8). The Fourier transform $\hat{T}(\omega_x, \omega_z)$ of $T(x, z)$ is the *transfer function* of the conventional CSLM. In appendix B we give expressions for $\hat{T}(\omega_x, 0)$ ((B.9) and (B.10)) and $\hat{T}(0, \omega_z)$ (B.11). We see that both functions have a logarithmic singularity at the origin due to the fact that $T(x, z)$ tends to zero rather slowly in the light zone, i.e. $|x| < |z|$ (see (A.7)). As a consequence $T(x, z)$ is not an integrable function of the two variables x, z.

The function $T(x, z)$, however, is not a realistic representation of the impulse response function of the microscope because it corresponds to the use, in the image plane, of a pinhole with a radius much smaller than the Rayleigh distance. This condition is never satisfied in practice because it would provide too small values of the signal-to-noise ratio. As a consequence the size of the pinhole is comparable with the Rayleigh distance even if this choice implies a loss of resolution.

On the other hand, in the super-resolving microscope based on the use of optical masks, the light distribution in the image plane is analysed by means of two masks and the light transmitted by these masks is integrated by a large detector [5, 6]. Therefore the signal-to-noise ratio always has an acceptable value in this case.

For these reasons, in order to estimate the effective improvement of resolution provided by the super-resolving CSLM, we must compare its transfer function with that of a conventional CSLM when realistic values of the size of the pinhole are used.

In our model, with 1D images, the use of the pinhole is equivalent to integration of the image over some interval $[-a, a]$. In such a case the impulse response function $T(x, z)$ must be replaced by the following one

$$T_a(x, z) = W(x, z) W_a(x, z)$$
$$W_a(x, z) = \frac{1}{2a} \int_{-a}^{a} W(x - x', z)\, dx'. \tag{5.1}$$

We have used a normalization such that $T_a(x, z) \to T_0(x, z) = T(x, z)$ in the limit $a \to 0$. Again, $\hat{T}_a(\omega_x, \omega_z)$ is the transfer function of the conventional CSLM with a pinhole of radius a.

By means of elementary but lengthy calculations the computation of $\hat{T}_a(\omega_x, \omega_z)$ can be reduced to the computation of 1D integrals over bounded intervals. We do not give the analytic expressions here, we only show the results in figure 4. We again obtain the well known effect that increasing the pinhole is equivalent to reducing the effective bandwidth of the instrument and therefore is equivalent to reducing its resolving power.

As proved in [4], the use of the optical mask (4.1) is equivalent to the use of a truncated singular-function expansion for estimating the unknown object. Moreover, thanks to the scanning procedure, we only need to evaluate this object at the confocal point,

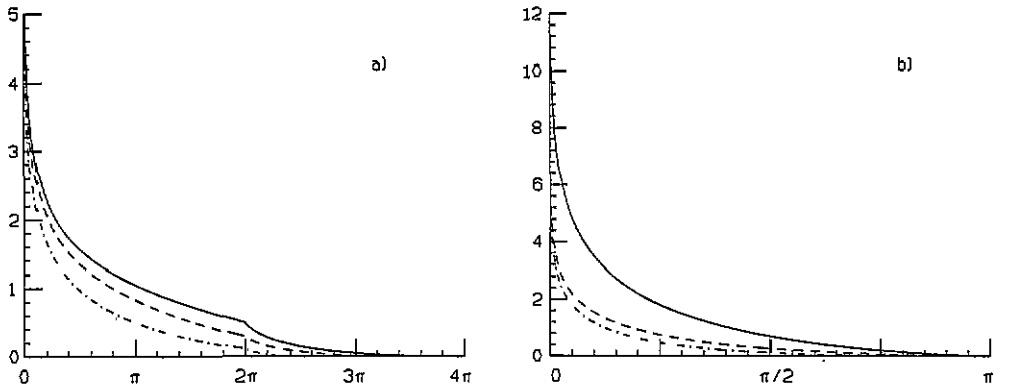

Figure 4. (*a*) The function $\hat{T}_a(\omega_x, 0)$ in the cases $a = 0$ (full curve), $a = 0.5$ (broken curve) and $a = 1$ (chain curve). (*b*) The functions $\hat{T}_a(0, \omega_z)$ in the cases $a = 0$ (full curve), $a = 0.5$ (broken curve) and $a = 1$ (chain curve).

i.e. $x' = 0, z' = 0$ [2,3]. If K is the number of terms in (4.1), then the estimated value of the object is

$$\tilde{f}^{(K)}(0,0) = \sum_{k=0}^{K-1} \frac{1}{\alpha_k} (g, v_k)_1 u_k(0,0). \tag{5.2}$$

Just by extending the proof given in [3], one can easily show that, if we neglect the noise contribution, then (5.2) can be written in the form

$$\tilde{f}^{(K)}(0,0) = \int_{-\infty}^{+\infty} dx' \int_{-\infty}^{+\infty} dz' \, T^{(K)}(x', z') f(x', z') \tag{5.3}$$

where $f(x', z')$ is the true object and

$$T^{(K)}(x', z') = \sum_{k=0}^{K-1} u_k(0,0) u_k(x', z'). \tag{5.4}$$

The function $T^{(K)}(x', z')$ is the *impulse response function* of the super-resolving scanning microscope and, as follows from the properties of the singular functions, it is band limited, with bandwidth interior to the region drawn in figure 1(*c*). The Fourier transform $\hat{T}^{(K)}(\omega'_x, \omega'_z)$ of $T^{(K)}(x', z')$ is the *transfer function* of the instrument and is given by

$$\hat{T}^{(K)}(\omega'_x, \omega'_z) = \sum_{k=0}^{K-1} u_k(0,0) \hat{u}_k(\omega'_x, \omega'_z) \tag{5.5}$$

where $\hat{u}_k(\omega'_x, \omega'_z)$ can be computed from (3.12) or (3.21).

In figure 5 we give the result of our computation of $\hat{T}_K(\omega_x, \omega_z)$ in the case $K = 34$, i.e. in the case of the mask of figure 3(*a*) which corresponds to the use of all the singular values greater than 10^{-2}. We do not give the result for $K = 125$ because it is rather similar to that shown in figure 5.

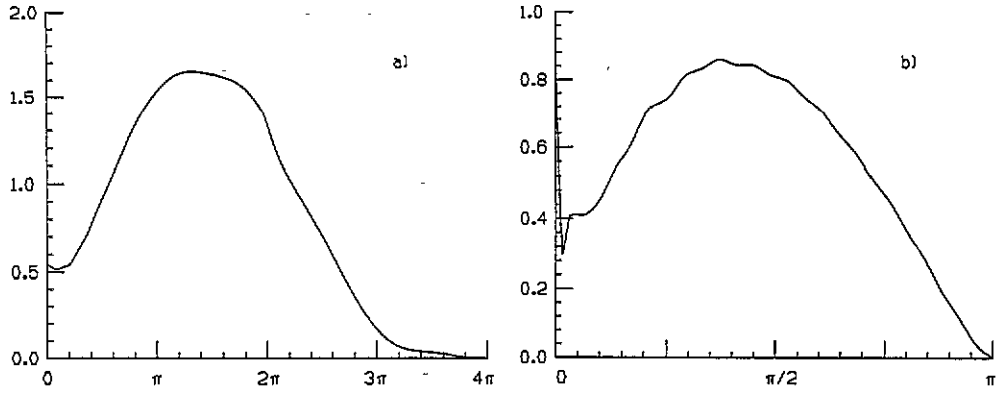

Figure 5. The function $\hat{T}_K(\omega_x, \omega_z)$ in the case $K = 34$. (*a*) The function $\hat{T}_K(\omega_x, 0)$. (*b*) The function $\hat{T}_K(0, \omega_z)$.

In order to compare the super-resolving CSLM, i.e. the microscope based on the use of the mask (4.1), with the conventional CSLM we must compare the transfer function of figure 5 with the transfer functions of figure 4. For this purpose it has been suggested in [9], that we compare the transfer functions one obtains by performing a regularized deconvolution of the images produced by the various microscopes. Then, as proved in [9], if $\hat{T}(\omega_x, \omega_z)$ is the transfer function of the microscope, the regularized image deconvolution is equivalent to a microscope with a transfer function given by

$$\hat{T}_\mu(\omega_x, \omega_z) = \frac{|\hat{T}(\omega_x, \omega_z)|^2}{|\hat{T}(\omega_x, \omega_z)|^2 + \mu} \tag{5.6}$$

where μ is the *regularization parameter*. Moreover, in [9] it is also shown that the effective band of the microscope corresponds to the spatial frequencies ω_x and ω_z such that $|\hat{T}_\mu(\omega_x, \omega_z)| \geqslant \frac{1}{2}$.

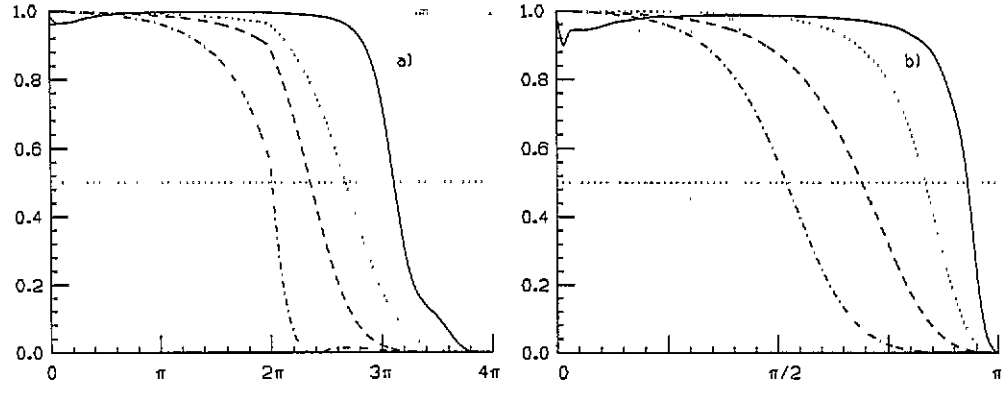

Figure 6. The regularized transfer functions with $\mu = 10^{-2}$ (μ = regularization parameter) for the super-resolving CSLM (full curves) and for the conventional CSLM with a pinhole $a = 0$ (dotted curves), $a = 0.5$ (broken curves) and $a = 1$ (chain curves). Part (*a*) shows $\hat{T}(\omega_x, 0)$ and part (*b*) $\hat{T}(0, \omega_z)$.

In figure 6 we compare the regularized transfer function (with $\mu = 10^{-2}$) of the super-resolving microscope with those of the conventional microscope for different values of the pinhole radius a. As we see the effective bandwidth of the super-resolving microscope (determined by the horizontal dotted line) is always broader than those of the conventional microscopes. This effect is especially evident in the case of the axial transfer function $\hat{T}_\mu(0, \omega_z)$ where the effective bandwidth of the super-resolving microscope practically coincides with the full bandwidth. Therefore the improvement of axial resolution is greater than the improvement of lateral resolution.

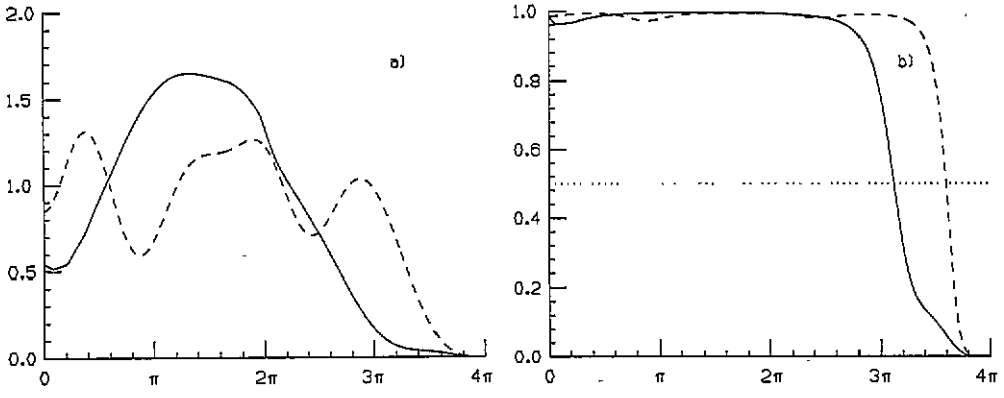

Figure 7. Lateral transfer functions of the super-resolving microscope for 2D objects (full curve) and 1D objects (broken curve). (*a*) Transfer functions corresponding to singular values greater than 10^{-2}. (*b*) The regularization of the previous transfer functions with a value of the regularization parameter $\mu = 10^{-2}$.

Finally, in figure 7 the lateral transfer function of the 2D super-resolving microscope is compared with the lateral transfer function of the 1D super-resolving microscope discussed in [2]. In both cases only the singular values greater than 10^{-2} are used, i.e. 34 singular values for the 2D case and 7 singular values for the 1D case. As indicated by the horizontal dotted line in figure 7(*b*), the effective bandwidth for 1D objects is greater than the effective bandwidth for 2D objects. This result is not surprising; as we remarked in section 4 the inversion of the image by assuming that the object is 1D means that *a priori* knowledge about the object has been used. Therefore we expect that the lateral resolution of 1D objects is better than the lateral resolution of 2D objects, since the use of *a priori* knowledge in general implies an improvement of resolution.

Appendix A

In this appendix we derive the main properties of the function

$$S(x, z) = \tfrac{1}{2} \int_{-1}^{1} \exp\{-i\pi(xt + \tfrac{1}{2}zt^2)\}\, dt \tag{A.1}$$

whose modulus is an even function of both variables

$$|S(x, z)| = |S(-x, z)| = |S(x, -z)| = |S(-x, -z)|. \tag{A.2}$$

A first remark is that this function is the solution of the following Cauchy problem for the Schrödinger 'time-dependent' equation (the 'time' being the axial variable z)

$$\begin{aligned} &\mathrm{i}\frac{\partial}{\partial z}S(x,z) = -\frac{1}{2\pi}\frac{\partial^2}{\partial x^2}S(x,z) \\ &S(x,0) = \operatorname{sinc}(x). \end{aligned} \tag{A.3}$$

Therefore, from general properties of the Schrödinger equation it follows that, for any z, we have

$$\int_{-\infty}^{+\infty} W(x,z)\,\mathrm{d}x = \int_{-\infty}^{+\infty} |S(x,z)|^2\,\mathrm{d}x = \int_{-\infty}^{+\infty} \operatorname{sinc}^2(x)\,\mathrm{d}x = 1 \tag{A.4}$$

$W(x,z)$ being defined as in (1.3). This means that, in any plane orthogonal to the optical axis, the total intensity is equal to one. Another consequence, which can also be derived directly from (A.1), is that the Fourier transform of $S(x,z)$, denoted by $\hat{S}(\omega_x,\omega_z)$, is a line-mass concentrated over an arc of a parabola (ω_x,ω_z are the spatial frequencies associated, respectively, with the lateral variable x and the axial variable z). More precisely we have

$$\hat{S}(\omega_x,\omega_z) = 2\pi \operatorname{rect}\left(\frac{\omega_x}{\pi}\right)\delta\left(\omega_z + \frac{1}{2\pi}\omega_x^2\right) \tag{A.5}$$

where

$$\operatorname{rect}(t) = \begin{cases} 1 & |t| \leqslant 1 \\ 0 & |t| > 1. \end{cases} \tag{A.6}$$

The support of (A.5) is plotted in figure 1.

The main purpose of this appendix, however, is to derive the following asymptotic bounds on the function $S(x,z)$

$$\text{(a)} \qquad |S(x,z)| \leqslant \frac{C_1}{\sqrt{|z|}} \qquad |z| \geqslant |x| \tag{A.7}$$

$$\text{(b)} \qquad |S(x,z)| \leqslant \frac{C_2}{|x|} \qquad |z| \leqslant |x| \tag{A.8}$$

where C_1, C_2 are suitable constants. Notice that the domains in (a) and (b) correspond, respectively, to the light and shadow regions of geometrical optics.

In order to derive (a), let us first remark that, thanks to (A.2), we can assume $z > 0$. Moreover we put

$$\tan\vartheta = \frac{x}{z} \qquad |\tan\vartheta| \leqslant 1 \tag{A.9}$$

and, by introducing the variable $u = \sqrt{\pi z}(t + \tan\vartheta)$, from (A.1) we get

$$S(x,z) = \frac{1}{2\sqrt{\pi z}} \mathrm{e}^{\mathrm{i}\pi z(\tan\vartheta)^2/2} \int_{-(1-\tan\vartheta)\sqrt{\pi z}}^{(1+\tan\vartheta)\sqrt{\pi z}} \mathrm{e}^{-\mathrm{i}u^2/2}\,\mathrm{d}u. \tag{A.10}$$

Let us now split the integration domain into the two segments $[0, (1+\tan\vartheta)\sqrt{\pi z}]$ and $[-(1-\tan\vartheta)\sqrt{\pi z}, 0]$. We can write

$$S(x,z) = \frac{1}{2\sqrt{\pi z}} e^{i\pi z(\tan\vartheta)^2/2} \left\{ \int_0^{(1+\tan\vartheta)\sqrt{\pi z}} e^{-iu^2/2}\,du + \int_0^{(1-\tan\vartheta)\sqrt{\pi z}} e^{-iu^2/2}\,du \right\} \tag{A.11}$$

and, by recalling the value of the Fresnel integral

$$\int_0^{+\infty} e^{-iu^2/2}\,du = \tfrac{1}{2}\sqrt{2\pi} e^{-i\pi/4} \tag{A.12}$$

we obtain

$$S(x,z) = \frac{1}{\sqrt{2z}} e^{i\pi z(\tan\vartheta)^2/2 - i\pi/4} - \frac{1}{2\sqrt{\pi z}} e^{i\pi z(\tan\vartheta)^2/2} \left\{ \int_{(1+\tan\vartheta)\sqrt{\pi z}}^{+\infty} e^{-iu^2/2}\,du + \int_{(1-\tan\vartheta)\sqrt{\pi z}}^{+\infty} e^{-iu^2/2}\,du \right\}. \tag{A.13}$$

Now, the function of z and $\tan\vartheta$ defined by the two integrals between the braces is a bounded and continuous function of the two variables for $z \in [0, \infty]$ and $\tan\vartheta \in [-1, 1]$. Therefore the representation (A.13) implies the bound (A.7).

In order to derive (b), i.e. the bound (A.8), we notice that the integral (A.1) can be written in the form

$$S(x,z) = \int_{-1}^{1} f(t) e^{ixS(t)}\,dt \tag{A.14}$$

with $S(t) = -\pi t$. Since $S'(t) \neq 0$, we can use the following asymptotic expansion for $x \to \infty$, z fixed [11]

$$S(x,z) \sim \frac{1}{ix} e^{i\pi x} \sum_{n=0}^{\infty} a_n(z)(ix)^{-n} - \frac{1}{ix} e^{-i\pi x} \sum_{n=0}^{\infty} b_n(z)(ix)^{-n} \tag{A.15}$$

where

$$a_n(z) = \frac{1}{2\pi^{n+1}} \frac{d^n}{dt^n} e^{-i\pi z t^2/2}\bigg|_{t=-1} \tag{A.16}$$

$$b_n(z) = \frac{1}{2\pi^{n+1}} \frac{d^n}{dt^n} e^{-i\pi z t^2/2}\bigg|_{t=1} \tag{A.17}$$

From these expressions one derives that

$$a_n = P_n(-i\tfrac{1}{2}\pi z) e^{-i\pi z/2} \qquad b_n = P_n(i\tfrac{1}{2}\pi z) e^{-i\pi z/2} \tag{A.18}$$

where $P_n(t)$ denotes a polynomial of degree n. Therefore all the coefficients of the expansion (A.15) are bounded functions of x and z when $|z| \leqslant |x|$ and x is large. This remark implies the bound (A.8).

We conclude by noticing that the leading term in the expansion (A.15) is given by

$$S(x,z) \sim \operatorname{sinc}(x) e^{-i\pi z/2} \tag{A.19}$$

and therefore it coincides, except for the phase factor $\exp(-i\pi z/2)$, with $S(x, 0)$.

Appendix B

In this appendix we investigate the Fourier transforms of the functions

$$W(x,z) = |S(x,z)|^2 \tag{B.1}$$

and

$$T(x,z) = |W(x,z)|^2 = |S(x,z)|^4. \tag{B.2}$$

The Fourier transform of $S(x,z)$ is given in (A.5).

We first consider the Fourier transform of $W(x,z)$ as a function of x for fixed z, i.e.

$$\tilde{W}(\omega_x, z) = \int_{-\infty}^{+\infty} e^{-ix\omega_x} W(x,z)\,dx. \tag{B.3}$$

Since we have $W(-x,z) = W(x,z)$, we also have $\tilde{W}(-\omega_x, z) = \tilde{W}(\omega_x, z)$. Then, for $\omega_x > 0$, using (A.5) and the convolution theorem we obtain

$$\tilde{W}(\omega_x, z) = \frac{1}{2\pi}\,\mathrm{rect}\left(\frac{\omega_x}{2\pi}\right)\int_{-\pi}^{\pi-\omega_x} e^{i(z/\pi)\omega_x t}\,dt. \tag{B.4}$$

The integral can be easily computed. Using again the symmetry property mentioned above, we obtain the following result

$$\tilde{W}(\omega_x, z) = \mathrm{rect}\left(\frac{\omega_x}{2\pi}\right)\frac{\sin\left[|\omega_x|(1-(1/2\pi)|\omega_x|)z\right]}{|\omega_x|z}. \tag{B.5}$$

In particular this implies that, for any z, $W(x,z)$ is a band limited function of x, with bandwidth 2π.

It is easy now to Fourier transform (B.5) with respect to the z variable. The result is the Fourier transform of $W(x,z)$, which is given by

$$\hat{W}(\omega_x, \omega_z) = \frac{\pi}{|\omega_x|}\,\mathrm{rect}\left(\frac{\omega_x}{2\pi}\right)\mathrm{rect}\left[\frac{\omega_z}{|\omega_x|\left(1-(1/2\pi)|\omega_x|\right)}\right]. \tag{B.6}$$

Therefore the support of $\hat{W}(\omega_x, \omega_z)$ is the domain interior to the contour consisting of the following four parabolic arcs (see figure 1)

$$|\omega_z| = |\omega_z|\left(1 - \frac{1}{2\pi}|\omega_x|\right) \qquad |\omega_x| \leqslant 2\pi. \tag{B.7}$$

Using properties of the support of the convolution product, one can derive from (B.6) that the support of the Fourier transform of $T(x,z) = |W(x,z)|^2$ is the domain interior to the following contour (see figure 1)

$$|\omega_z| = \max\left\{1 - \frac{1}{4\pi}|\omega_x|^2,\ |\omega_x|\left(1 - \frac{1}{4\pi}|\omega_x|\right)\right\} \qquad |\omega_x| \leqslant 4\pi. \tag{B.8}$$

The Fourier transform of the function $T(x,z)$ (B.2) can be computed using the relationship $\hat{T} = (2\pi)^{-2}\hat{W} * \hat{W}$ and the expression (B.6) for $\hat{W}$. By means of elementary but

lengthy calculations, one can find the following expressions for the restrictions of $\hat{T}(\omega_x, \omega_z)$ to the ω_x and ω_z axis

$$\hat{T}(\omega_x, 0) = \left(1 - \frac{1}{2\pi}|\omega_x|\right)(2\ln 2 - 1) + \frac{1}{4\pi}|\omega_x| + \left(1 + \frac{1}{2\pi}|\omega_x|\right)\ln\left(\frac{2\pi + |\omega_x|}{2|\omega_x|}\right)$$
$$|\omega_x| \leqslant 2\pi \tag{B.9}$$

$$\hat{T}(\omega_x, 0) = \left(1 - \frac{1}{4\pi}|\omega_x|\right) - \left(1 - \frac{1}{2\pi}|\omega_x|\right)\ln\left(1 + \frac{|\omega_x| - 4\pi}{|\omega_x|}\right)$$
$$2\pi \leqslant |\omega_x| \leqslant 4\pi \tag{B.10}$$

$$\hat{T}(0, \omega_z) = \ln\left(\frac{\pi}{|\omega_z|}\right) + 2\ln\left(1 + \sqrt{1 - \frac{|\omega_z|}{\pi}}\right) - 2\sqrt{1 - \frac{|\omega_z|}{\pi}} \qquad 0 \leqslant |\omega_z| \leqslant \pi. \tag{B.11}$$

The function $\hat{T}(\omega_x, \omega_z)$ has a logarithmic singularity at the origin. This is related to the fact that the function $T(x, z)$ is not integrable as a consequence of its slow decay at infinity in the light zone of geometrical optics, i.e. $|z| \geqslant |x|$ (see (A.7) and the bound on $\sigma(z)$, equation (2.4), implied by this inequality).

References

[1] Bertero M, Brianzi P and Pike E R 1987 Super-resolution in confocal scanning microscopy *Inverse Problems* **3** 195–212

[2] Bertero M, Boccacci P, Defrise M, De Mol C and Pike E R 1989 Super-resolution in confocal scanning microscopy: II. The incoherent case *Inverse Problems* **5** 441–61

[3] Bertero M, Boccacci P, Davies R E and Pike E R 1991 Super-resolution in confocal scanning microscopy: III. The case of circular pupils *Inverse Problems* **7** 655–74

[4] Bertero M, Boccacci P, Davies R E, Malfanti F, Pike E R and Walker J G 1992 Super-resolution in confocal scanning microscopy: IV. Theory of data inversion by the use of optical masks *Inverse Problems* **8** 1–23

[5] Young M R, Jiang S H, Davies R E, Walker J G, Pike E R and Bertero M 1992 Experimental confirmation of super-resolution in coherent confocal scanning microscopy using optical masks *J. Microsc.* **165** 131–8

[6] Grochmalicki J, Pike E R, Walker J G, Bertero M, Boccacci P and Davies R E 1993 Superresolving masks for incoherent scanning microscopy *J. Opt. Soc. Am.* A **10** 1074–7

[7] Wijnaends van Resandt R W, Marsman H J B, Kaplan R, Davoust J, Stelzer E H K and Shicker R 1985 Optical fluorescence microscopy in three dimensions: microtomoscopy *J. Microsc.* **138** 29–34

[8] Brakenhoff G J, van der Voort H T M, van Sprosen E A and Nanninga N 1986 Three-dimensional imaging by confocal scanning fluorescence microscopy *Ann. NY Acad. Sci.* **483** 405–15

[9] Bertero M, Boccacci P, Brakenhoff G J, Malfanti F and van der Voort H T M 1990 Three-dimensional image restoration and super-resolution in fluorescence confocal microscopy *J. Microsc.* **157** 3–20

[10] Born M and Wolf E 1959 *Principles of Optics* (Oxford: Pergamon)

[11] Sidorov Yu V, Fedoryuk M V and Shabunin M I 1985 *Lectures on the Theory of Functions of a Complex Variable* (Moscow: Mir) pp 410–1